Article

Cobalt, Ferrum Co-Doped Ni_3Se_4 Nano-Flake Array: An Efficient Electrocatalyst for the Alkaline Hydrogen Evolution and Overall Water Splitting

Chuancang Zhou [1], Hongyu Wu [1,*], Feipeng Zhang [2] and Yigao Miao [1]

[1] College of Technology, Lishui University, Lishui 323000, China; zhouchuancang@163.com (C.Z.); myg8627@gmail.com (Y.M.)

[2] College of Science, Henan University of Urban Construction, Pingdingshan 467036, China; zhfp@emails.bjut.edu.cn

*   Correspondence: wuhongyu@lsu.edu.cn

Abstract: Herein, Co, Fe co-doped Ni_3Se_4 nano-flake array $((Ni_{0.62}Co_{0.35}Fe_{0.03})_3Se_4)$ was prepared on conductive carbon cloth by a two-step hydrothermal method. XRD and EDX analysis show that the nanosheets are monoclinic Ni_3Se_4, and Co, and Fe were doped into the lattice of Ni_3Se_4. Electrochemical tests showed that Co, Fe co-doping can effectively improve the hydrogen evolution activity of Ni_3Se_4 in acidic and alkaline environment. When the current density of $(Ni_{0.62}Co_{0.35}Fe_{0.03})_3Se_4/CC$ is $10\ mA/cm^2$ in 1 M KOH solution, the overpotentials of hydrogen evolution and oxygen evolution are 87 mV and 53.9 mV, respectively, and the Tafel slopes are 122.6 and 262 mV/dec. The electrochemical active area test (ECSA) and the polarization curve test further show that $(Ni_{0.62}Co_{0.35}Fe_{0.03})_3Se_4/CC$ has a larger electrochemical active area $(34.8\ mF/cm^2)$, lower electrolytic potential (0.9 V at $10\ mA/cm^2$) and better stability. Therefore, the novel bifunctional catalyst synthesized by a simple method is a promising candidate for large-scale industrial water electrolysis.

Keywords: $(Ni_{0.62}Co_{0.35}Fe_{0.03})_3Se_4/CC$; nanosheet array; electrolytic water; hydrogen and oxygen evolution activity

1. Introduction

It is still a very important and challenging work to design and prepare bifunctional electrolyzed water catalysts with high activity and high stability. Herein, electrocatalytic water splitting to generate hydrogen is one of the most attractive sustainable technologies for the production of hydrogen energy due to the environment friendly, high purity, simple process [1]. The modularity of an electrolyzer is very suitable for the centralized production of hydrogen, and for combined use with renewable energy, such as photovoltaic and wind energy, and in particular the low-voltage power from garbage can be fully utilized. However, the high dependence on noble metal catalysts has greatly increased the cost of water electrolysis, which has become a bottleneck problem for hydrogen production from electrolytic water [2–5]. Therefore, the development of low-cost, high activity, high utilization of non-noble metal catalysts has become one of the most popular research directions in the field of electrolyzed water. In an acid or alkaline environment, high-efficiency non-noble metal catalysts with hydrogen and oxygen evolution simultaneously are very rare. Electrocatalysts for Overall Water Splitting mainly include transition metal phosphides, transition metal sulfides, transition metal selenides, layered double hydroxides, alloy materials, and so on [6–8]. Especially, in the alkaline environment, the hydrogen evolution activity of the catalyst is much worse than in the acidic environment. Alkaline hydrogen evolution electrocatalysts mainly include alloys, transition metal hydroxides, sulfides, selenides, carbides and phosphides [9–15], however, the hydrogen evolution activity, the double function catalytic performance of hydrogen evolution and the oxygen

evolution are mostly unsatisfactory. Among these, the conductivity of transition metal selenides is stronger than that of sulfide, and the ionization energy of selenium is smaller than that of sulfur. Therefore, in theory, transition metal selenides may exhibit more unique hydrogen evolution performance than metal sulfides. Compared with single metal selenides, electrocatalytic activity of bimetallic selenides is greatly improved due to bimetallic synergy and lattice defect. Therefore, in recent years, more and more researchers have begun to study the transition metal selenides with bimetallic or even three metals. By adjusting the proportion of metal, the electrolytic water activity may be improved. At present, the selenides catalysts for hydrogen evolution are mainly $CoSe_2$, $NiSe_2$ and NiSe [16–20], and mainly in powder state or load-on-nickel foam, so Ni_3Se_4 load on conductive carbon cloth has rarely been reported. Huang et al. [21] prepared a NiSe-Ni_3Se_2/RGO hybrid by the hydrothermal method. The overpotential (η^{10}) and Tafel slope of this material in 1 M KOH were 188 mV and 92 mV/dec, respectively. Tian et al. [22] prepared $NiSe/FeSe_2$ nanostructures by the hydrothermal method. In 1 M KOH, the oxygen evolution overpotential and the Tafel slope are 210 mV and 53.65 mV/dec, respectively. Electrocatalytic hydrogen evolution performance in these documents is not ideal, and the phase is relatively complex, which is not pure phase. The hybrid does not make the doped elements enter the lattice, does not cause defects on the molecular scale, and is just a simple mixing. Element doping into the lattice can distort the lattice and change the interaction between electrons, so as to expose more active sites and improve the electrocatalytic activity. Fan et al. [23] studied the electrocatalytic hydrogen and oxygen evolution and the total water hydrolysis properties of Co, Fe doped $NiSe_2$. Bimetallic ion doping Ni_3Se_4 needs further development.

In this paper, we report a Co, Fe doped Ni_3Se_4 electrocatalyst with nanoplate arrays loaded on carbon cloth (CC), prepared by the hydrothermal method. It exhibits high hydrogen evolution activity in an acidic and alkaline environment, oxygen evolution activity in an alkaline environment, and excellent performance of overall water splitting in an alkaline environment.

2. Experimental

After hydrothermal treatment for 4 h in 68% HNO_3 (Sinopharm Chemical Reagent Co., Ltd., Shanghai, China) at 120 °C, the carbon cloth with an area of 1 cm × 1 cm was cleaned and dried for use. $NiCoFe(OH)_X$ was prepared according to previous reports [24]. Carbon cloth was purchased from Taiwan Carbon Energy Co. Ltd. $Ni(NO_3)_2.6H_2O$, $Co(NO_3)_2.6H_2O$, $Fe(NO_3)_3.9H_2O$, NH_4F, $CO(NH_2)_2$, $NaBH_4$(Sinopharm Chemical Reagent Co., Ltd.), selenium power and KOH were purchased from Sinopharm Chemical Reagent Co. Ltd. All chemicals were used without further purification. The water used throughout all the experiments was purified through a deionization purification system. Typically, a 75 mL aqueous solution with 0.02 M of $Ni(NO_3)_2 \cdot 6H_2O$, 0.01 M $Co(NO_3)_2 \cdot 6H_2O$, 0.001 M $Fe(NO_3)_3.9H_2O$, 0.15 M NH_4F and 0.15 M $CO(NH_2)_2$ was prepared. Typically, 0.02 M $Ni(NO_3)_2 \cdot 6H_2O$, 0.01 M $Co(NO_3)_2 \cdot 6H_2O$, 0.001 M $Fe(NO_3)_3.9H_2O$, 0.15 M NH_4F and 0.15 M $CO(NH_2)_2$ were dissolved in 75 mL deionized water. After the solution was stirred for 10 min, treated carbon cloth was soaked in it and then heated at 120 °C for 24 h in the hydrothermal reactor. Then the reactor cooled to room temperature, after which the carbon cloths loaded with hydroxides were washed with DI water and anhydrous ethanol repeatedly. A light yellow-green thin layer of material loaded onto the carbon cloth was dried in an electric oven at 80 °C for 8 h. Then, 0.13 g $NaBH_4$ and 0.12 g Se powder were mixed and stirred with water and a certain amount of ethylene glycol for 2 h to obtain a light red liquid, and the volume ratio of water to ethylene glycol was 7:1. The carbon cloth loaded with the light yellow-green thin layer material was placed in the red liquid, and it was heated at 180 °C for 24 h in a hydrothermal reactor. The solution fullness in the hydrothermal reactor is 80%. After cooling, the carbon cloth loaded with selenides was washed repeatedly with ethanol and deionized water for several times, and then dried in a vacuum oven at 50 °C for 12 h.

XRD measurements were investigated by using a Dandong DX-2700B diffractometer (Dandong, China) CuKa radiation (λ = 1.5418 Å). SEM images and energy spectrum analysis were taken by a scanning electron microscopy (VEGA3, TESCAN, Brno city, Czech Republic). X-ray photoelectron spectroscopy (XPS) measurements were performed on a Thermo Fisher Scientific K-Alpha spectrometer (Waltham, MA, USA) using monochromatized Al Kα excitation. All binding energies were calibrated by using the contaminant carbon (C1S = 284.6 eV) as a reference.

All the electrochemical measurements were performed with a PARSTAT MC 2000 A workstation (Princeton Applied Research, Oak Ridge, USA). HER measurements were performed with three-electrode system in 0.5 M H_2SO_4 or 1 M KOH at 25 °C. The working electrode is carbon cloth loaded selenides film. The reference electrode is Ag/AgCl in acidic environment and Hg/HgO in alkaline environment. A carbon rod with a diameter of 0.5 cm was used as the counter electrode. Carbon rod electrode, Ag/AgCl and Hg/HgO electrodes were purchased from Tianjin Aida Technology Development Co. Ltd. (Tianjin, China). All the test potentials in this paper need to be converted to the potential relative to the reversible hydrogen electrode (RHE). Here, the working potentials were all converted to an RHE scale. The potential conversion formula of hydrogen evolution in acidic environment is as follows: η = E(Ag/AgCl) + 0.2224 V; the potential conversion formula of hydrogen evolution in alkaline environment is as follows: η = E(Hg/HgO) + 0.059 × pH + 0.098 V. The calculation formula of oxygen evolution overpotential in alkaline environment is as follows: η = $E_{measurement}$ + pH × 0.059 + 0.098 − 1.23 V. Nitrogen was continuously supplied throughout the electrochemical test. Linear scan voltammetry (LSV) measurements were carried out at a scan rate of 5 mV/s. The Tafel curves were obtained by drawing the logarithmic curve of overpotential and current density. The amplitude of electrochemical impedance test is 10 mV, the scanning frequency is 100 kHz–0.1 Hz, and the test voltage is non-Faraday District. The electrochemically active surface area (ECSA) of the catalysts is determined by calculating the electric double layer capacitance (C_{dl}) by means of the cyclic voltammetry curve (CV) test. The CV test was carried out at different scanning speeds of 20, 40, 60, 80 and 100 mV/s, and the voltage range was selected at non-Faraday District, which was near the positive starting voltage. The two electrodes system was used in the overall water electrolysis test, and the electrodes were the same film materials and were tested in 1 M KOH solution. All the measurements were corrected using iR compensation.

3. Results and Discussion

The photographs of the bare carbon cloth after nitric acid treatment, the carbon cloth depositing hydroxide and the selenide-coated carbon cloth are shown in Figure 1. It can be seen from the Figure that NiCoFe(OH)$_x$/CC is light green, $(Ni_{0.62}Co_{0.35}Fe_{0.03})_3Se_4$/CC is white brown, and the coating is evenly distributed on the carbon cloth. The scanning electron microscopy (SEM) images and energy dispersive X-ray diffraction (EDX) spectrum of the prepared films are shown in Figure 2. It can be seen from the picture that the carbon fiber is tightly wrapped by nanoflake grain. The diameter of the carbon fiber is about 10–20 μm, and the diameter of the coated carbon fiber is about 20–30 μm. The thickness of the nanoflake is less than 50 nm, the size of it is less than 5 μm, the size and thickness of the nanoflake are uniform and close-packed. Due to the nanoflake cross growth, there are a large number of nano or micron open holes on the coated carbon fiber surface. The energy spectrum analysis of the nanoflake in the different positions shows that the chemical element composition is uniform and the molar ratio of Ni:Co:Fe:Se = 10.25:5.8:0.58:20.11. X-ray diffraction (XRD) of the nanoflake film (Figure 3) indicates that the nanoflake has the characteristic peak of monoclinic Ni_3Se_4, the PDF card number of it is 18-0890, space group I2/M (12), cell parameters are 6.22 Å, 3.63 Å, 10.52 Å, 90°, 90.53°, 90°. Co or Fe compounds have not been detected, which indicates that Co, Fe has been doped into Ni_3Se_4 lattice. About 30.14° and 43.17° shown in the Figure 3 are $NiSe_2$ or elemental selenium. It shows that there are some heterophases in Ni_3Se_4, but the crystal phase in $(Ni_{0.6}Co_{0.4})_3Se_4$ is relatively pure, and there are few heterophases, indicating that Co has

completely entered the Ni_3Se_4 lattice. Moreover, $(Ni_{0.62}Co_{0.35}Fe_{0.03})_3Se_4$ has less impurities and is basically pure phase. From the position of the peak in each spectrum, the position of the main peak shifted to the left, and the crystallinity increased with the increase in doped elements. The large doping amount of cobalt is due to the large similarity of atomic radius and properties between the two, which can be doped with high concentration. However, the chemical properties of iron are quite different from nickel, and the valence states are variable, Therefore, low concentration doping is often used, and high concentration doping can easily cause the appearance of impurity phase.
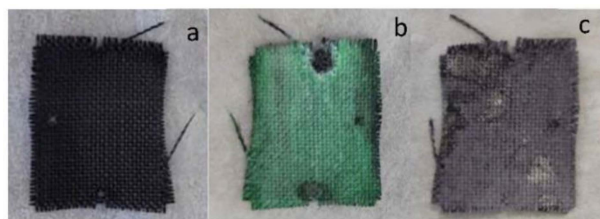
Figure 1. Appearance photos of bare carbon cloth (**a**); $(Ni_{0.62}Co_{0.35}Fe_{0.03})(OH)_X/CC$ (**b**); $(Ni_{0.62}Co_{0.35}Fe_{0.03})_3Se_4/CC$ (**c**).
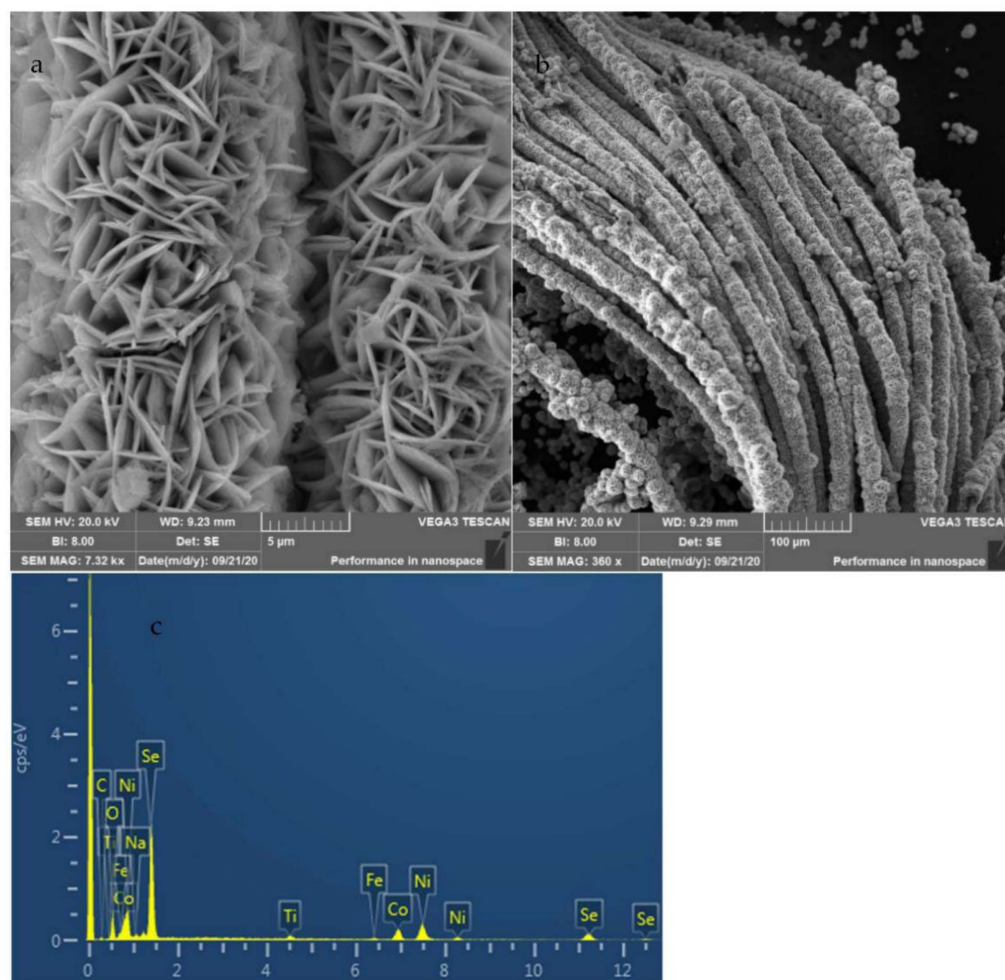
Figure 2. SEM image (**a**,**b**) and EDX spectrum (**c**) of $(Ni_{0.62}Co_{0.35}Fe_{0.03})_3Se_4/CC$.
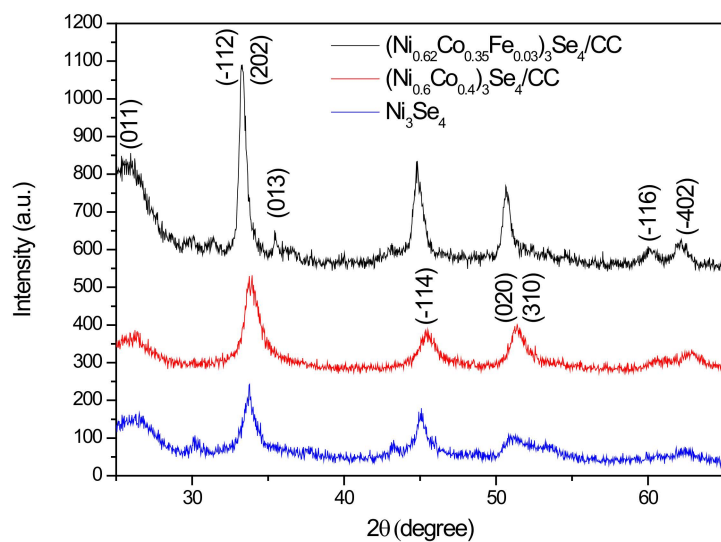
Figure 3. XRD pattern of $(Ni_{0.62}Co_{0.35}Fe_{0.03})_3Se_4$/CC, $(Ni_{0.6}Co_{0.4})_3Se_4$/CC, Ni_3Se_4/CC.
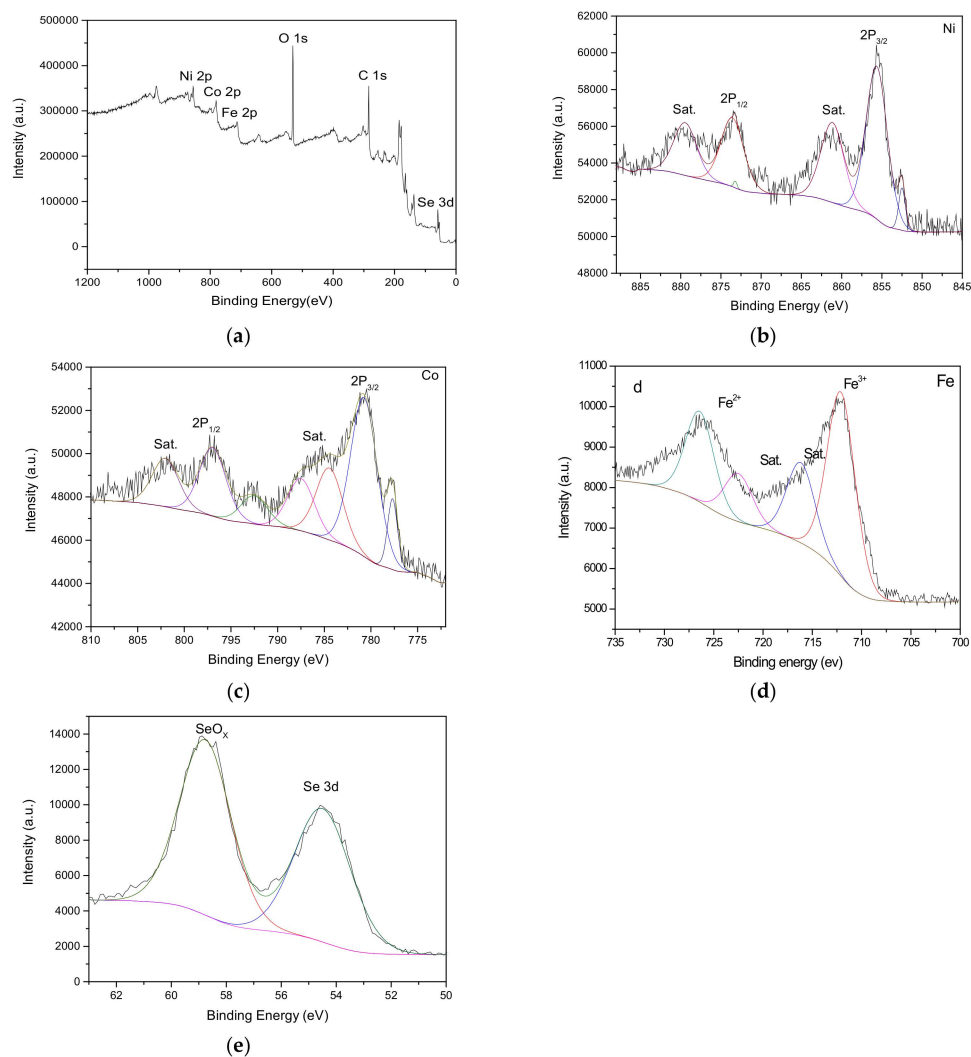
Figure 4. (**a**) XPS survey of $(Ni_{0.62}Co_{0.35}Fe_{0.03})_3Se_4$/CC; (**b**) Ni 2p; (**c**) Co 2p; (**d**) Fe 2p; and (**e**) Se 3d XPS spectra of $(Ni_{0.62}Co_{0.35}Fe_{0.03})_3Se_4$/CC.

X-ray photoelectron spectroscopy is performed to analyze the surface element composition and elemental valence states of $(Ni_{0.62}Co_{0.35}Fe_{0.03})_3Se_4/CC$. The survey XPS spectrum (Figure 4) clearly reveals the existence of the Ni, Co, Fe, Se, O, and C elements, which is consistent with the above elemental mapping results. The fitting results of Ni2p peaks show that the positions 873.7 and 855.6 eV with binding energy correspond to the spin orbits of 2p1/2 and 2p3/2, respectively, and there is a shakeup satellite peak at positions 861 and 879 eV. The co2p peak fitting results show that the energy level orbits at 780.89 and 797 eV are 2p3/2 and 2p1/2, respectively, and 784, 787 and 802 eV are satellite peaks, respectively. The 778 eV peak of cobalt should correspond to metallic cobalt. The appearance of metal state increases the conductivity of the catalyst, enriches the electronic state, and improves the catalytic activity. The fitting of Fe2p shows that 711 and 724.3 eV are the energy levels of 2p3/2 and 2p1/2, respectively, and 718.7 corresponds to the satellite peak. The peak at the binding energy of 54.5 eV corresponds to Se 3d orbit, moreover, due to the re exposure of the sample to air, the element Se on the sample surface is oxidized, and a large SeO_X peak can be observed. All the above characterization directly or indirectly proved the successful synthesis of $(Ni_{0.62}Co_{0.35}Fe_{0.03})_3Se_4$.

The polarization curve, Tafel curve, ECSA, and I-t curve of $(Ni_{0.62}Co_{0.35}Fe_{0.03})_3Se_4/CC$, Ni_3Se_4/CC in 1 M KOH are shown in Figure 5. The results demonstrate that the overpotential of $(Ni_{0.62}Co_{0.35}Fe_{0.03})_3Se_4/CC$ and Ni_3Se_4/CC is 87 and 107 mV at 10 mA/cm^2 of current density, respectively, which is better than the overpotential 96 and 100 mV of NiSe/NF and Ni_3Se_2/CF (NF is Ni foam, CF is carbon fiber) reported before [25,26]. The bare carbon cloth has almost no hydrogen evolution activity. The Tafel slopes of $(Ni_{0.62}Co_{0.35}Fe_{0.03})_3Se_4/CC$, Ni_3Se_4 were 122.6 and 114 mV/dec, respectively. The Tafel slope was independent of the number of active sites, only related to the type of active sites. The rate—determining step in the process of hydrogen evolution is Volmer step, and the desorption reaction should be Heyrovsky step, that is, the adsorption of hydrogen atoms combined with hydrogen ions in the solution. In order to further investigate the catalytic activity, electrochemical active surface area (ECSA) was studied. The electrochemical double-layer capacitance (C_{dl}) was calculated by measuring the CV curves in potential voltage range of non-Faraday District (The potential range relative to Hg/HgO is $-0.36 \sim -0.46$ V) at different scanning speeds. Figure 5c,d shows the cyclic voltametric curves of $(Ni_{0.62}Co_{0.35}Fe_{0.03})_3Se_4/CC$, Ni_3Se_4/CC in 1 M KOH at different scanning speeds of 20, 40, 60, 80 and 100 mV/s, by calculating the slope of the linear relationship between current density and scanning speed at a certain potential, the electrochemical double layer capacitance(C_{dl}) is 34.8 and 30 mF/cm^2, respectively. The larger C_{dl} indicated that the more active sites were exposed, the more the area of electrochemical activity increased. It suggested that the appropriate amount of Co, Fe doping can improve the catalytic activity. The stability of the catalyst for hydrogen evolution was further tested. Hydrogen evolution reaction carried out for a long time under 1.5 V voltage in 1 M KOH by chronoamperometry (I-t). The results indicate that the current remained stable for more than 20 h. The current density decreases from 0 to 5 h, because the surface powder falls off due to the impact of gas. The chemical changes of active components and the closure of porous structure led to the decrease of catalytic activity. The current density changes little and tends to be stable after 5–14 h. After 14 h, the current density increases gradually, which may be due to the compound action of some NiCoFe(OH)x and metal-selenides under the long-term action of strong alkali, Doping or heterostructure produces defects, which increases the activity of hydrogen evolution. The specific reasons need to be further verified by the experiment. Hydrogen evolution reaction (HER) polarization curves and Tafel curves of $(Ni_{0.62}Co_{0.35}Fe_{0.03})_3Se_4/CC$ and Ni_3Se_4/CC in 0.5 M H_2SO_4 solution are shown in the Figure 6. When the current density is 10 mA/cm^2, over-potential of $(Ni_{0.62}Co_{0.35}Fe_{0.03})_3Se_4/CC$ and Ni_3Se_4/CC are 50 mV and 114 mV, respectively, which shows that Co, Fe doping can improve electrocatalytic activity in acid solution. The Tafel slopes of $(Ni_{0.62}Co_{0.35}Fe_{0.03})_3Se_4/CC$ and Ni_3Se_4/CC were 111 and 171 mV/dec, respectively, which indicated that the control step was Volmer step and the hydrogen evolution

route was Volmer-Heyrovsky [27,28]. The above results show that Co, Fe doping can improve the hydrogen evolution activity of Ni_3Se_4/CC in acid solution more than in alkaline solution. From Table 1, we can see the electrocatalytic hydrogen evolution characteristics of different nickel selenide phases and different cations doped on different substrates. It can be seen that the performance of the doped phase is better than that of the pure phase, and the performance of the cation double doping is slightly higher than that of single ion doping. We believe that the nanoporous structure can provide a higher active area and is more conducive to ion transport and gas desorption. Moreover, due to the lattice distortion and the synergistic effect of Ni, Co, Fe, its catalytic activity is enhanced. In addition, compared with undoped, the stronger electronic interaction also optimizes the adsorption and desorption of hydrogen. We propose that this enhancement is correlated with the lattice distortion and strong electronic interaction between the metal cations. According to reference [23,27–29], due to heteroatom displacement defects, doped iron can not only provide additional opportunities to optimize electronic conductivity, but also create more active sites. Finally, compared with undoped $NiSe_2$, iron-doped nano dendrite $NiSe_2$ shows excellent OER properties. A total of 6% of iron doping showed the best OER performance.
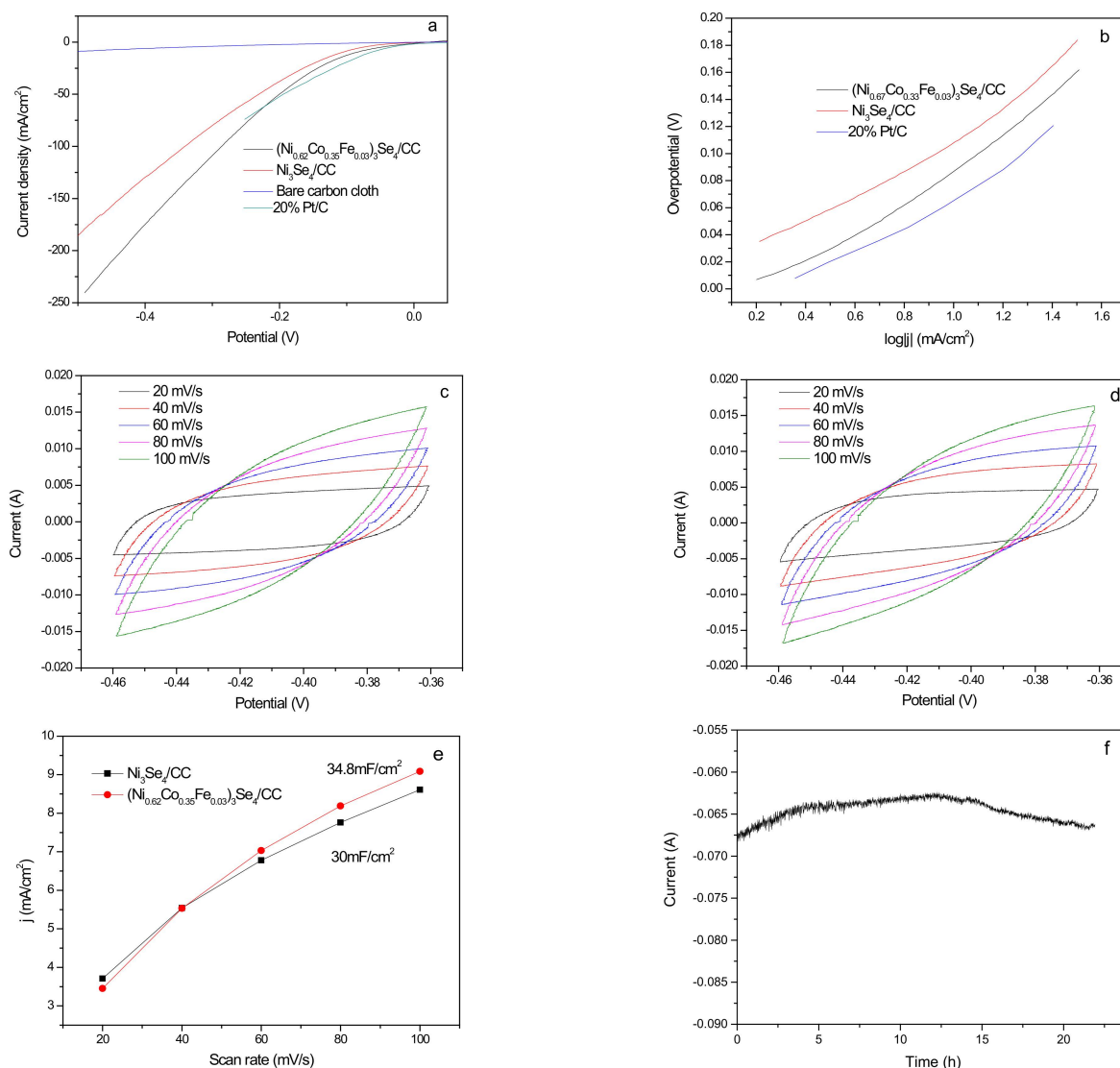
Figure 5. (**a**) HER LSV curves of $(Ni_{0.62}Co_{0.35}Fe_{0.03})_3Se_4$/CC, Ni_3Se_4/CC; (**b**) corresponding Tafel plots; (**c**,**d**) CV curves at different scanning speeds; (**e**) The estimated C_{dl} of $(Ni_{0.62}Co_{0.35}Fe_{0.03})_3Se_4$/CC, Ni_3Se_4/CC; (**f**) Chronopotentiometry of $(Ni_{0.62}Co_{0.35}Fe_{0.03})_3Se_4$/CC (1.5 V relative to hydrogen electrode). All tests were performed in 1 M KOH electrolyte.
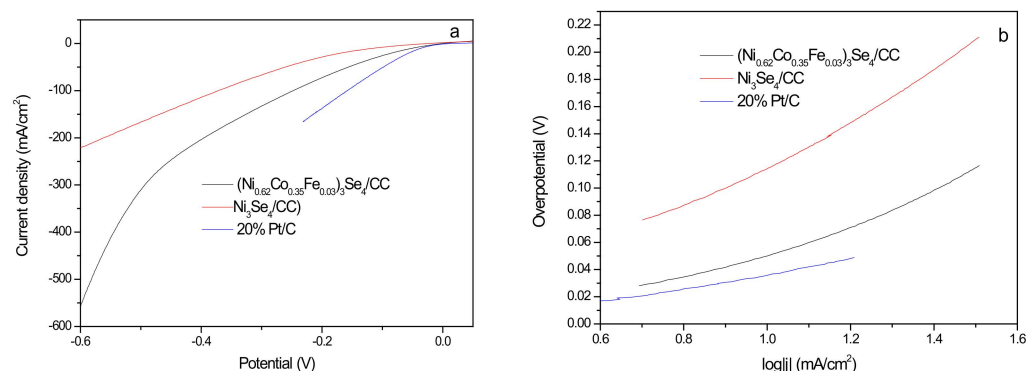
Figure 6. (**a**) HER LSV curves of $(Ni_{0.62}Co_{0.35}Fe_{0.03})_3Se_4/CC$, Ni_3Se_4/CC in 0.5 M H_2SO_4; (**b**) corresponding Tafel plots.

Table 1. Benchmarking the Metal (Fe, Co, Ni) Selenides with Respect to the HER overpotential at 10 mA/cm² (η10) in 1 M KOH.

Catalyst	η^{10} (mV)	Tafel Slope (mV/dec)	Ref
$Co_{0.13}Ni_{0.87}Se_2/Ti$	64	63	[28]
$NiSe/NF$	96	120	[25]
Ni_3Se_2/CF	100	98	[26]
$Fe_{0.09}Co_{0.13}$-$NiSe_2/CFC$	63	89	[29]
$(Ni_{0.62}Co_{0.35}Fe_{0.03})_3Se_4/CC$	87	122.6	In this paper

It can be seen from the polarization curve of oxygen evolution (Figure 7) that overpotentials of $(Ni_{0.62}Co_{0.35}Fe_{0.03})_3Se_4/CC$ and Ni_3Se_4/CC are 53.9 and 62.5 mV, respectively, when the current density is 10 mA/cm². The overpotential is 318 and 640 mv at 100 mA/cm². The corresponding tafel slopes are 262 and 278 mV/dec, which multiplied compared with hydrogen evolution. Thus, the Tafel slopes suggested that the mass transport step is rate-limiting for OER. It shows that the electrochemical discharge step of oxygen evolution is slow and is the control step of the whole electrolysis water reaction. The oxygen evolution activity of the bare carbon cloth is very low. The oxygen evolution reaction involves many electrochemical unit steps, and the reaction reversibility is poor. There are double Tafel regions in the oxygen evolution reaction. The slope of Tafel in the low potential area is small, and the slope in the high potential area is larger, which may be due to the change of electrode surface state, and another control step has appeared, so we chose the potential interval with a straight line in the middle. By comparing the Tafel slope of oxygen evolution, it can be seen that Co, Fe doping does not change the reaction route and control steps of Ni_3Se_4/CC oxygen evolution. The stability of $(Ni_{0.62}Co_{0.35}Fe_{0.03})_3Se_4/CC$ as the oxygen evolution electrode was investigated by means of chronoamperometry curves (I-t) at 1.5 V relative to hydrogen electrode. The current decreased slightly within 15 h, and remained stable between 15–20 h.

As shown in Figure 8, it is the impedance spectrum of $(Ni_{0.62}Co_{0.35}Fe_{0.03})_3Se_4/CC$ and Ni_3Se_4/CC in 1 M KOH or in 0.5 M H_2SO_4. In the analog circuit diagram, RS is the resistance between counter electrode and working electrode and between solutions. RP is the electrochemical polarization impedance, which is affected by reaction kinetics and reactant diffusion. According to the formula $ZCPE = 1/[(j\omega)NY_0]$, for different N values, Y_0 represents different element, which represents the non-ideal state of the electrode surface and its roughness. When the dispersion effect exists on the electrode surface, the N value ranges from 1 to 0.5. The closer N is to 1, the closer it is to the pure electric double layer capacitor, which indicates doping improves the electrode surface smoothness. Doping makes the polarization resistance decrease and the N value of the constant phase element increase, which indicates an increase in the surface compactness. Although the resistance decreases, the diffusivity decreases, so the Tafel slope does not change much.

The results of hydrogen evolution and oxygen evolution at three electrodes in alkaline solution show that $(Ni_{0.62}Co_{0.35}Fe_{0.03})_3Se_4$/CC shows excellent performance as a bifunctional electrode for water electrolysis. In order to further simulate the catalytic performance of $(Ni_{0.62}Co_{0.35}Fe_{0.03})_3Se_4$/CC in the electrolytic water industry, the overall water splitting test is performed in a two-electrode system by using $(Ni_{0.62}Co_{0.35}Fe_{0.03})_3Se_4$/CC as both cathode and anode. As shown in Figure 9a, $(Ni_{0.62}Co_{0.35}Fe_{0.03})_3Se_4$/CC and Ni_3Se_4/CC only need a cell voltage of 0.9 and 0.93 V, respectively when the current density reaches 10 mA/cm^2 in 1 M KOH. Such activity is better than that of most previously reported metal selenides catalysts [13]. The two- electrode chronoamperometry test (I-t) was carried out under a constant 1.5 V voltage, its current decreased slightly within 20 h, and still maintained high activity and stability.
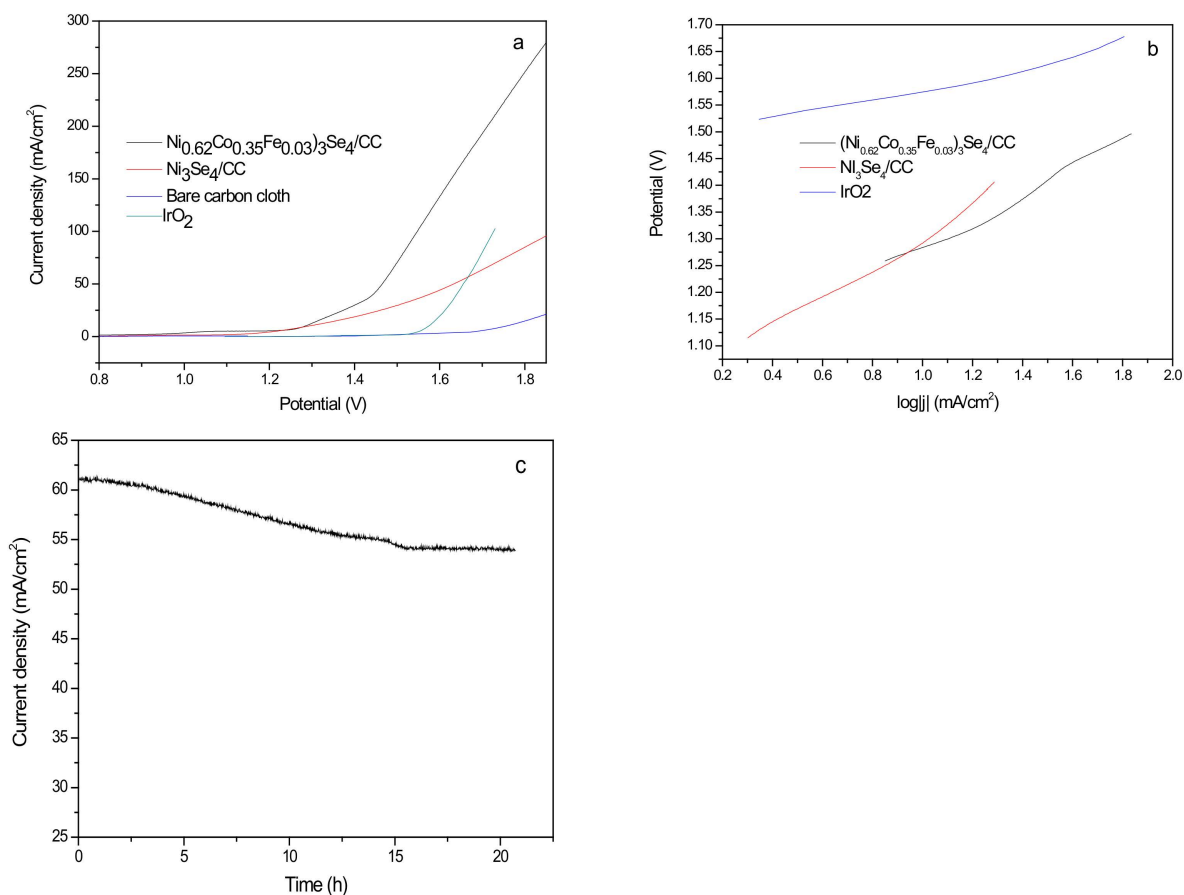
Figure 7. (**a**) OER LSV curves of $(Ni_{0.62}Co_{0.35}Fe_{0.03})_3Se_4$/CC, Ni_3Se_4/CC; (**b**) corresponding Tafel plots; (**c**) Chronopotentiometry of $(Ni_{0.62}Co_{0.35}Fe_{0.03})_3Se_4$/CC. All tests were performed in 1 M KOH electrolyte, relative to RHE 1.5 V.
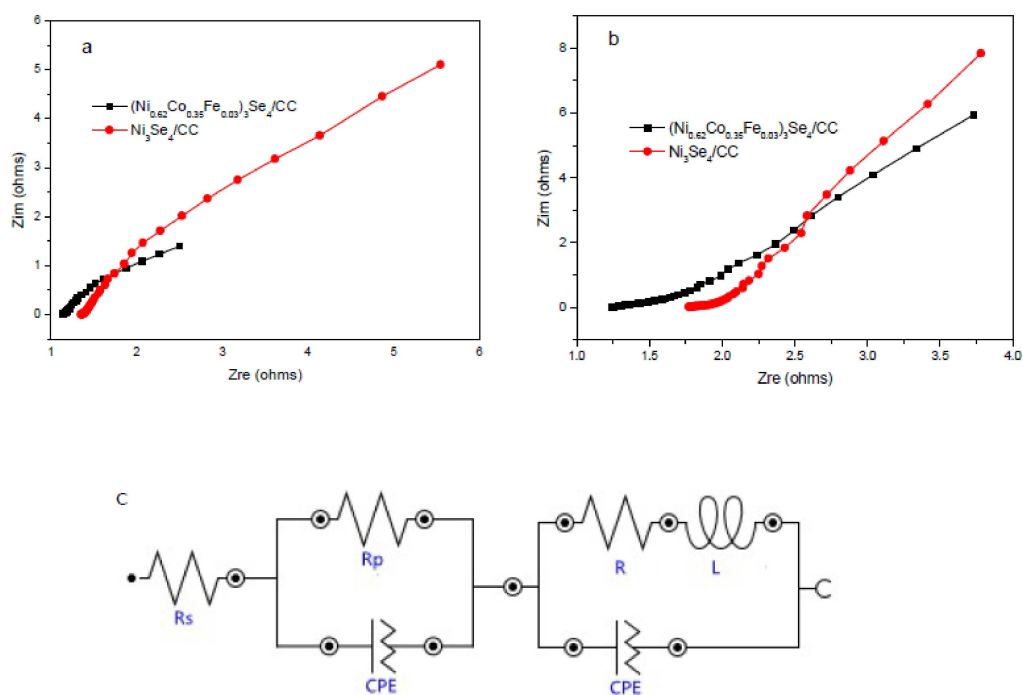
Figure 8. EIS diagram of $(Ni_{0.62}Co_{0.35}Fe_{0.03})_3Se_4/CC$, Ni_3Se_4/CC In acidic (**a**); alkaline solutions (**b**); and analog circuit diagram (**c**).
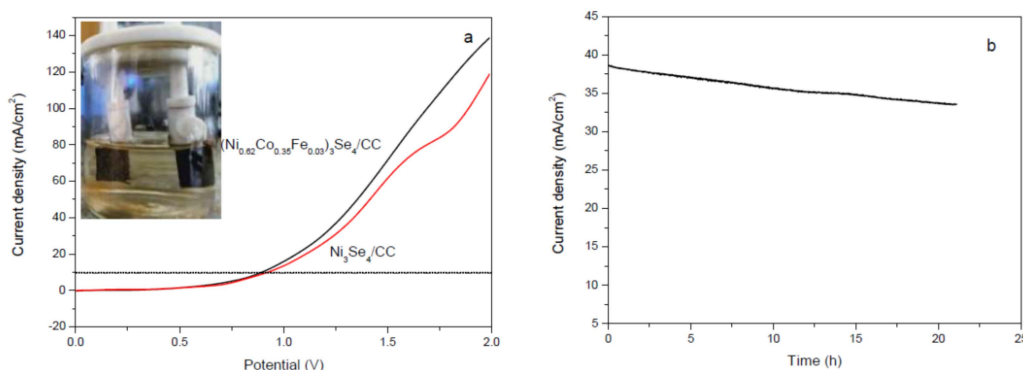
Figure 9. (**a**) Polarization curves of overall water splitting at a scan rate of 10 mV/s in 1 M KOH solution; (**b**) chronoamperometry measurements for stability of $(Ni_{0.62}Co_{0.35}Fe_{0.03})_3Se_4/CC$ as electrode pairs using overall water splitting at 1.5 V.

4. Conclusions

$(Ni_{0.62}Co_{0.35}Fe_{0.03})_3Se_4/CC$ and Ni_3Se_4/CC nanoflake arrays were prepared on carbon cloth by means of a two-step hydrothermal method. The thickness of the nanoflake is less than 50 nm, and the molar ratio of Ni:Co:Fe:Se = 10.25:5.8:0.58:20.11. XRD analysis shows that the nanoflake is monoclinic pure phase Ni_3Se_4, Co, Fe has been doped into the Ni_3Se_4 lattice to replace the position of Ni. The hydrogen evolution overpotential of $(Ni_{0.62}Co_{0.35}Fe_{0.03})_3Se_4/CC$ and Ni_3Se_4/CC are 87 and 107 mV (10 mA/cm^2), respectively, the corresponding Tafel slopes are 122.6 and 114 mV/dec. The oxygen evolution overpotentials are 53.9 and 62.5 mV (10 mA/cm^2), respectively, and the corresponding Tafel slopes are 262 and 278 mV/dec in 1 M KOH. The hydrogen evolution overpotential of $(Ni_{0.62}Co_{0.35}Fe_{0.03})_3Se_4/CC$ and Ni_3Se_4/CC in 0.5 M H_2SO_4 are 50 and 114 mV, respectively, and the Tafel slope is 111 and 171 mV/dec. These results indicate that $(Ni_{0.62}Co_{0.35}Fe_{0.03})_3Se_4/CC$ and Ni_3Se_4/CC are excellent bifunctional electrocatalysts for oxygen and hydrogen evolution. The two-electrode polarization curve (LSV) in 1 M KOH

shows that the voltage required for $(Ni_{0.62}Co_{0.35}Fe_{0.03})_3Se_4/CC$ and Ni_3Se_4/CC is about 0.9 and 0.93 V when the current density reaches 10 mA/cm^2. Under the voltage of 1.5 V, the current density remained stable within 20 h. The low price and excellent performance of $(Ni_{0.62}Co_{0.35}Fe_{0.03})_3Se_4/CC$ indicate that it has commercial value as an electrocatalyst for Overall Water Splitting, which provides more ideas and directions for the research and industrialization of electrolytic water.

Author Contributions: Conceptualization, C.Z.; Methodology, C.Z. and H.W.; investigation, C.Z. and Y.M.; writing—original draft preparation, C.Z.; writing—review and editing, C.Z. and F.Z. All authors have read and agreed to the published version of the manuscript.

Institutional Review Board Statement: Ethical approval is not required.

Informed Consent Statement: Informed consent was obtained from all subjects involved in the study.

Data Availability Statement: The datasets generated during and/or analyzed during the current study are available from the corresponding author on reasonable request.

Conflicts of Interest: Authors declare that they have no known competing financial interests or personal relationships that could have appeared to influence the work reported in this paper.

References

1. Fang, Z.-W.; Peng, L.-L.; Qian, Y.-M.; Zhang, X.; Xie, Y.-J.; Cha, J.-J.; Yu, G.-H. Dual Tuning of Ni-Co-A (A = P, Se, O) Nanosheets by Anion Substitution and Holey Engineering for Efficient Hydrogen Evolution. *J. Am. Chem. Soc.* **2018**, *140*, 5241–5247. [CrossRef] [PubMed]
2. Björketun, M.E.; Karlberg, G.S.; Rossmeisl, J.; Chorkendorff, I.; Wolfschmidt, H.; Stimming, U.; Nørskov, J.K. Hydrogen evolution on Au(111) covered with submonolayers of Pd. *Phys. Rev. B Condens. Matter* **2011**, *84*, 045407. [CrossRef]
3. Grigoriev, S.A.; Millet, P.; Fateev, V.N. Evaluation of carbon-supported Pt and Pd nanoparticles for the hydrogen evolution reaction in PEM water electrolysers. *J. Power Sources* **2008**, *177*, 281–285. [CrossRef]
4. Pluntke, Y.; Kibler, L.A.; Kolb, D.M. Unique activity of Pd monomers: Hydrogen evolution at AuPd(111) surface alloys. *Phys. Chem. Chem. Phys.* **2008**, *10*, 3684–3688. [CrossRef]
5. Chorbadzhiyska, E.; Mitov, M.; Hristov, G.; Dimcheva, N.; Nalbandian, L.; Evdou, A.; Hubenova, Y. Pd-Au electrocatalysts for hydrogen evolution reaction at neutral pH. *Int. J. Electrochem.* **2014**, *2014*, 239270. [CrossRef]
6. Guo, D.-Y.; Wang, J.-H.; Zhang, L.; Chen, X.-A.; Wan, Z.-X.; Xi, B. Strategic Atomic Layer Deposition and Electrospinning of Cobalt Sulfde/Nitride Composite as Efcient Bifunctional Electrocatalysts for Overall Water Splitting. *Small* **2020**, *16*, 2002432. [CrossRef]
7. Feng, J.-R.; Lv, F.; Zhang, W.Y.; Li, P.H.; Wang, K.; Yang, C.; Wang, B.; Yang, Y.; Zhou, J.H.; Lin, F.; et al. Iridium-Based Multimetallic Porous Hollow Nanocrystals for Efcient Overall-Water-Splitting Catalysis. *Adv. Mater.* **2017**, *29*, 1703798. [CrossRef]
8. Zhang, B.; Zhu, C.; Wu, Z.; Stavitski, E.; Lui, Y.H.; Kim, T.-H.; Francisco, J.S. Integrating Rh Species with NiFe-Layered Double Hydroxide for Overall Water Splitting. *Nano. Lett.* **2020**, *20*, 136–144. [CrossRef]
9. Ye, S.-H.; Luo, F.-Y.; Xu, T.-T.; Zhang, P.-Y.; Shi, H.-D.; Qin, S.Q.; Wu, J.P.; He, C.X.; Ouyang, X.P.; Zhang, Q.-L.; et al. Boosting the alkaline hydrogen evolution of Ru nanoclusters anchored on B/N–doped graphene by accelerating water dissociation. *Nano Energy* **2020**, *68*, 104301. [CrossRef]
10. Ling, T.; Zhang, T.; Ge, B.-H.; Han, L.-L.; Zheng, L.R.; Lin, F.; Xu, Z.R.; Hu, W.-B.; Du, X.-W.; Davey, K.; et al. Well-Dispersed Nickel- and Zinc-Tailored Electronic Structure of a Transition Metal Oxide for Highly Active Alkaline Hydrogen Evolution Reaction. *Adv Mater.* **2019**, *31*, e1807771. [CrossRef]
11. Zhang, H.; Yu, L.; Chen, T.; Zhou, W.; Lou, X.-W. Surface Modulation of Hierarchical MoS$_2$ Nanosheets by Ni Single Atoms for Enhanced Electrocatalytic Hydrogen Evolution. *Adv. Funct. Mater.* **2018**, *28*, 1807086. [CrossRef]
12. Hou, C.-C.; Cao, S.; Fu, W.-F.; Chen, Y. Ultrafine CoP Nanoparticles Supported on Carbon Nanotubes as Highly Active Electrocatalyst for Both Oxygen and Hydrogen Evolution in Basic Media. *ACS Appl. Mater. Interfaces* **2015**, *7*, 28412–28419. [CrossRef] [PubMed]
13. Zhong, W.-W.; Xiao, B.-B.; Lin, Z.-P.; Wang, Z.-P.; Huang, L.-G.; Shen, S.-J.; Zhang, Q.-H.; Gu, L. RhSe$_2$: A Superior 3D Electrocatalyst with Multiple Active Facets for Hydrogen Evolution Reaction in Both Acid and Alkaline Solutions. *Adv. Mater.* **2021**, *33*, 2007894. [CrossRef] [PubMed]

14. Wang, Z.P.; Lin, Z.-P.; Deng, J.; Shen, S.J.; Meng, F.Q.; Zhang, J.T.; Zhang, Q.H.; Zhong, W.W.; Gu, L. Elevating the d-Band Center of Six-Coordinated Octahedrons in Co9S8 through Fe-Incorporated Topochemical Deintercalation. *Adv. Energy Mater.* **2021**, *11*, 2003023. [CrossRef]

15. Lin, Z.P.; Shen, S.J.; Wang, Z.P.; Zhong, W.-W. Laser ablation in air and its application in catalytic water splitting and Li-ion battery. *iScience* **2021**, *24*, 102469. [CrossRef]

16. Gao, Z.; Qi, J.; Chen, M.; Zhang, W.; Cao, R. An Electrodeposited NiSe for Electrocatalytic Hydrogen and Oxygen Evolution Reactions in Alkaline Solution. *Electrochim. Acta* **2017**, *224*, 412–418. [CrossRef]

17. Jiang, K.; Liu, B.; Luo, M.; Ning, S.; Peng, M.; Zhao, Y.; Tan, Y. Single platinum atoms embedded in nanoporous cobalt selenide as electrocatalyst for accelerating hydrogen evolution reaction. *Nat. Commun.* **2019**, *10*, 1743. [CrossRef]

18. Zhong, W.-W.; Wang, Z.-P.; Gao, N.; Huang, L.-G.; Lin, Z.-P.; Liu, Y.P.; Meng, F.Q.; Deng, J.; Jin, S.F.; Zhang, Q.H.; et al. Coupled Vacancy Pairs in Ni-Doped CoSe for Improved Electrocatalytic Hydrogen Production Through Topochemical Deintercalation. *Angew. Chem. Int. Ed.* **2020**, *59*, 22743. [CrossRef]

19. Shen, S.-J.; Lin, Z.P.; Song, K.; Wang, Z.P.; Huang, L.G.; Yan, L.H.; Meng, F.Q.; Zhang, Q.H.; Gu, L.; Zhong, W.-W. Reversed active sites boost the intrinsic activity of graphene-like cobalt selenide for hydrogen evolution. *Angew. Chem. Int. Ed.* **2021**, *60*, 12360–12365. [CrossRef]

20. Lin, Z.-P.; Xiao, B.B.; Wang, Z.P.; Shen, S.J.; Huang, L.G.; Zhang, J.T.; Meng, F.Q.; Zhang, Q.H.; Gu, L.; Zhong, W.-W. Planar-coordination PdSe2 nanosheets as highly active electrocatalyst for hydrogen evolution reaction. *Adv. Funct. Mater.* **2021**, *31*, 2102321. [CrossRef]

21. Zhu, M.; Zhang, D.; Lu, Q.; Yan, Y.; Zhu, K.; Huang, X.M.; Wang, G. Hollow hexagonal NiSe–Ni3Se2 anchored onto reduced graphene oxide as efficient electrocatalysts for hydrogen evolution in wide-pH range. *Int. J. Hydrogen Energy* **2021**, *46*, 20524–20533. [CrossRef]

22. Zhai, X.; Pang, X.; Wang, X.; Tian, L. Facile fabrication of hydrangea-like NiSe/FeSe2 nanostructures towards efficient water oxidation. *J. Saudi Chem. Soc.* **2022**, *26*, 101469. [CrossRef]

23. Sun, Y.; Xu, K.; Wei, Z.; Li, H.; Fan, H.J. Strong Electronic Interaction in Dual-Cation-Incorporated NiSe2 Nanosheets with Lattice Distortion for Highly Efficient Overall Water Splitting. *Adv. Mater.* **2018**, *30*, 1802121. [CrossRef] [PubMed]

24. Yuan, C.; Yang, L.; Hou, L.; Li, D.; Shen, L.; Zhang, F.; Zhang, X. Synthesis and supercapacitance of flower-like Co(OH)2 hierarchical superstructures self-assembled by mesoporous nanobelts. *J. Solid State Electrochem.* **2012**, *16*, 1519–1525. [CrossRef]

25. Tang, C.; Cheng, N.; Pu, Z.; Xing, W.; Sun, X. NiSe Nanowire Film Supported on Nickel Foam: An Efficient and Stable 3D Bifunctional Electrode for Full Water Splitting. *Angew. Chem. Int. Ed.* **2015**, *54*, 9351–9355. [CrossRef] [PubMed]

26. Pu, Z.; Luo, Y.; Asiri, A.M.; Sun, X. Efficient Electrochemical Water Splitting Catalyzed by Electrodeposited Nickel Diselenide Nanoparticles Based Film. *ACS Appl. Mater. Interfaces* **2016**, *8*, 4718–4723. [CrossRef]

27. Jing, F.; Lv, Q.-Y.; Wang, Q.-J.; Chi, K.; Xu, Z.-Y.; Wang, X.-B.; Wang, S. Self-supported 3D porous N-Doped nickel selenide electrode for hydrogen evolution reaction over a wide range of pH. *Electrochim. Acta* **2019**, *304*, 202–209. [CrossRef]

28. Liu, T.; Asiri, A.M.; Sun, X. Electrodeposited Co-doped NiSe2 nanoparticles film: A good electrocatalyst for efficient water splitting. *Nanoscale* **2016**, *8*, 3911–3915. [CrossRef]

29. Zhou, J.; Yuan, L.-W.; Wang, J.W.; Xu, J. Combinational modulations of NiSe2 nanodendrites by phase engineering and iron-doping towards an efficient oxygen evolution reaction. *J. Mater. Chem. A* **2020**, *8*, 8113–8120. [CrossRef]